Information Integration and Communication in Heterogeneous Internet of Things: A Stochastic Geometry-Based Analytical Modeling*

Yulei Wang[a,b,c], Li Feng[a,*], Yalin Liu[c] and Zhongjie Li[b]

[a] School of Computer Science and Engineering, Macau University of Science and Technology, Macau 999078, China

[b] Hubei Key Laboratory of Intelligent Wireless Communications, Hubei Engineering Research Center of Intelligent Internet of Things Technology, College of Electronics and Information Engineering, South-Central Minzu University, Wuhan 430074, China

[c] School of Science and Technology, Hong Kong Metropolitan University, Hong Kong 999077, China

ARTICLE INFO

Keywords:
Device-to-device communication
Guard zone
Heterogeneous Internet of Things
In-band full-duplex
Poisson hole process
Stochastic geometry

ABSTRACT

The heterogeneous Internet of Things (HetIoT), consisting of densely coexisted cellular and device-to-device (D2D) devices, has become a foundational component of 5th generation and beyond networks. Considering the high density of devices, guard zones around base stations (BSs) are introduced to mitigate interference with each other. However, previous studies neglect the impact of cellular devices on D2D transmissions, which is also crucial in HetIoT. To address this issue, this paper presents the use of guard zones around both transmitting BSs and cellular devices. By leveraging a stochastic geometry approach, a novel spatial distribution model is constructed to effectively capture the location randomness and interdependencies between BSs, cellular, and D2D devices. Based on this spatial model, an analytical model is developed to derive expressions for the successful transmission probabilities of BSs, cellular, and D2D devices. This model accounts for the inherent randomness and interrelations between cellular and D2D transmissions, while also characterizing the complex mutual interference resulting from the two types of guard zones. Extensive Monte Carlo simulations confirm the high accuracy of the proposed theoretical model. This analytical model provides practical guidance for practitioners in selecting suitable parameter configurations to enhance performance in HetIoT.

1. Introduction

1.1. Background

In the era of 5th generation (5G) and beyond 5G (B5G) technologies, the growing demand for the Internet of Things (IoT) is driving an exponential increase in the number of connected IoT devices, expected to reach 55 to 80 billion by 2025 [1, 2, 3]. These devices have become ubiquitous, deployed across a wide range of applications including smart cities, environmental monitoring, industrial automation [4], security systems [5], advanced manufacturing [6], and intelligent transportation [7], as illustrated in Fig. 1. They continuously sense and collect various types of data—industrial, environmental, and personal—while transmitting, exchanging, and integrating these data for further processing, significantly enhancing daily lives. Furthermore, 5G/B5G technologies are anticipated to support nearly 10 million devices per km^2 outdoors and $1,000$ devices per 100 m^2 indoors [5]. Consequently, it is foreseeable that different IoT devices under diverse communication networks will coexist, thus forming a heterogeneous IoT (HetIoT) system [4, 8].

An HetIoT system integrates various communication networks, including cellular-enabled IoT networks (e.g., LTE-M [9] and NB-IoT [10]) and self-organized Device-to-Device (D2D) networks (e.g., Zigbee [11] and WiFi HaLow [12]). HetIoT devices encompass a wide range of machines and sensors supported by these diverse networks, such as wearable devices and monitoring sensors. To sum up, IoT devices primarily operate in two categories of networks: cellular networks and D2D networks. We refer to HetIoT devices operating in these two networks as cellular devices and D2D devices, respectively.

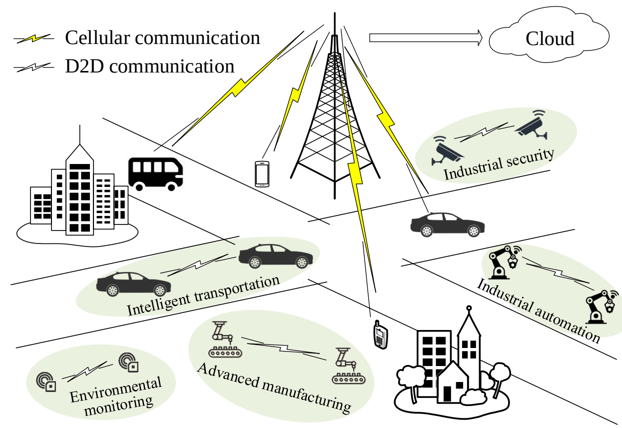

Figure 1: The architecture of information integration and communication in a typical HetIoT.

In a typical HetIoT system, IoT devices can reuse the licensed cellular spectrum to communicate with one another, either with or without the involvement of base stations (BSs) and the core network. Additionally, unlike the traditional half-duplex (HD) mode, where devices can either transmit or

*The work of L. Feng is funded by the Science and Technology Development Fund, Macau SAR under Grants 0093/2022/A2, 0076/2022/A2, and 0008/2022/AGJ. The work of Y. Liu is supported by the Hong Kong Metropolitan University Research Grant (Research and Development Fund) under Grant RD/2023/2.22.

*Corresponding author

ylwang@mail.scuec.edu.cn, ylwang@hkmu.edu.hk (Y. Wang); lfeng@must.edu.mo (L. Feng); ylliu@hkmu.edu.hk (Y. Liu); lizhongjie@mail.scuec.edu.cn (Z. Li)

receive signals at any given time, advancements in hardware have enabled devices to operate in in-band full-duplex (FD) mode, allowing simultaneous transmission and reception of signals on the same time/frequency resource blocks [13, 14]. Undoubtedly, as the two emerging innovations in 5G/B5G, the integration of D2D communication and FD technology holds significant promise for improving spectrum efficiency and enhancing network capacity [15]. However, the inherent broadcast nature of the wireless medium means that large-scale D2D communication can lead to substantial inter-network interference. Moreover, since both cellular and D2D devices are often randomly distributed in space, these mutual interferences exhibit notable spatial randomness and are influenced by location-dependent factors such as large- and small-scale fading. Therefore, effective interference management strategies are crucial for achieving higher system performance in such environments.

To effectively manage interference, establishing *guard zones* (also known as exclusion zones) is a widely adopted strategy across various network types. *A guard zone is typically defined as a circular region with a fixed radius around each transmitter, within which other devices are prohibited from transmitting*. This setup ensures sufficient spatial separation to mitigate mutual interference by inhibiting potential concurrent transmissions. In the context of HetIoT, which incorporate both cellular and D2D transmissions, although previous studies have primarily focused on establishing guard zones around BSs to alleviate interference from cellular transmissions [16], there is a growing recognition of the significant impact that interference from large-scale D2D transmissions can have on cellular communications (i.e., the footnote of [17]). Thus, integrating guard zones around both BSs and cellular devices is essential, considering the interactions between cellular and D2D devices. This comprehensive approach is necessary to ensure effective interference management within HetIoT.

1.2. Motivation

Despite advancements in integrating guard zones around both BSs and cellular devices, as well as the flexible deployment of D2D communications with devices operating in either HD or FD mode, implementing these features in HetIoT introduces significant complexities and randomness in terms of interference and spatial distribution. To address this issue, stochastic geometry—a powerful analytical tool that provides a probabilistic framework for modeling spatial point processes—has emerged as an effective method for capturing the intricate spatial configurations of wireless networks [18, 19]. Although stochastic geometry has been applied to cellular and D2D scenarios separately, limited research has explored their interactions in the context of guard zones.

In this study, we aim to fill the gap by leveraging stochastic geometry to analyze system performance in HetIoT. In particular, we need to characterize the spatial distributions of BSs, cellular devices, and D2D devices and analyze critical performance metrics in HetIoT. However, to achieve this goal, we need to overcome the following challenges:

- Firstly, the combination of D2D communication with in-band FD capabilities enables simultaneous transmission and reception, significantly enhancing spectral efficiency. However, as the number of D2D devices adopting FD communication increases, the resulting interference can degrade the performance of cellular communication. Therefore, it is crucial to *develop an effective FD mode selection strategy that efficiently mitigates D2D interference by regulating the number of D2D devices utilizing in-band FD communication.*

- Secondly, while establishing guard zones around BSs can effectively reduce interference from cellular transmissions, the impact of large-scale D2D transmissions on cellular communications cannot be overlooked. Thus, *integrating guard zones around both transmitting BSs and cellular devices offers a promising approach to alleviating overall system interference.*

- Finally, the random nature of cellular transmissions leads to the formation of random guard zones around transmitting BSs and cellular devices, which subsequently contributes to random D2D transmissions. *This randomness complicates the modeling of the spatial distribution of cellular and D2D devices, their interdependencies, and the complexity of various spatial interferences.*

Modeling and analyzing the performance of an HetIoT requires jointly considering the aforementioned factors. However, existing analytical models often fall short of capturing all these complexities comprehensively [13, 14, 17, 20]. This gap motivates us to develop a novel analytical modeling that accurately analyzes performance and offers configuration insights to enhance overall system efficiency.

1.3. Our contributions

Consider a typical HetIoT, characterized by: 1) densely coexisting cellular and D2D devices; 2) guard zones established around randomly distributed BSs and cellular devices; and 3) D2D devices that can operate in either FD or HD mode for D2D transmissions. Within this context, we build a stochastic geometry-based analytical model to investigate information integration and communication in this network, and theoretically analyze the successful transmission probabilities (STPs) for both cellular and D2D transmissions. Taking all these factors into account, the key contributions of this study are summarized as follows:

- *Establish a novel spatial distribution model for HetIoT.* The majority of previous work simply models the spatial distribution of BSs, cellular, and D2D devices by two homogeneous Poisson point processes (HPPPs) [13, 14]. However, their work cannot model the accurate network topology of our focused HetIoT with transmission probabilities and guard zones aroud transmitting devices. Our work applies thinning and approximation operations to HPPPs to cater to the probabilities in transmitting devices. Moreover, we use the superposition of two Poisson hole processes (PHPs) to model the activated D2D devices outside two distinct types of guard zones. This spatial model enables a precise and realistic representation of the network topology.

- *Develop a comprehensive analytical model for HetIoT.* The developed analytical model derives accurate expressions for the STPs of both cellular and D2D transmissions, incorporating critical system parameters such as the densities of transmitting cellular devices, D2D devices in HD/FD mode, and the guard zone radius. This model allows us to capture the inherent randomness and interdependencies of cellular and D2D transmissions, as well as the complex spatial interferences within the network.

- *Conduct extensive simulations for verification.* Extensive Monte Carlo simulations are conducted, which confirm the accuracy of the analytical modeling. These simulation results provide valuable insights for practitioners (e.g., network operators or engineers) in selecting suitable parameter configurations to enhance performance in HetIoT.

The rest of this paper is organized as follows. Section 2 reviews the related work. Section 3 presents the system model of the HetIoT. Section 4 derives a stochastic geometry-based analytical model for three STPs in the HetIoT. Section 5 validates the accuracy of the theoretical model through extensive Monte Carlo simulations. Finally, Section 6 concludes this paper and presents some discussions.

2. Related Work

The HetIoT, encompassing large-scale cellular and D2D devices, has emerged as a critical component in 5G/B5G networks. Extensive research has been conducted on the performance modeling and analysis of HetIoT, addressing various aspects such as covertness and secrecy [5, 21], resource allocation [22, 23], duplex mode selection [13, 14], and interference management (e.g., via guard zone), among others. In this context, the focus of this work is primarily on the existing literature on performance modeling in HetIoT, particularly studies that explore HD/FD-based and guard zone-based approaches, with an emphasis on distinguishing their differences.

2.1. Performance modeling of HetIoT in HD/FD

In HetIoT, full-duplex technology enables devices to simultaneously transmit and receive signals on the same time/frequency resource blocks, thereby improving spectrum efficiency. In this context, previous literature considers two modes of full-duplex technology in HetIoT devices, i.e., HD and FD modes. In [24, 25], the authors investigate an HetIoT composed of HD D2D and cellular devices, employing a stochastic geometry approach to model the spatial randomness of these devices and analyze the success probabilities for both cellular and D2D links. However, their models are not applicable to scenarios where D2D devices operate with random HD/FD mode selection. In [13], they propose a fine-tuned selection criterion for HD/FD mode operation in networks where D2D and cellular devices coexist. They develop a stochastic geometry-based model to calculate the outage probabilities of cellular and D2D devices. Similarly, Badri et al. in [14] analyze the interference experienced by cellular users from D2D devices using a stochastic geometry approach, where each D2D device can optimally choose between HD and FD mode to ensure the quality of service for cellular users.

Although the above studies consider HD/FD mode selection devices for spectrum efficiency and model HetIoT in stochastic geometry. However, they cannot solve the interference issues among cellular and D2D transmissions. This is also a crucial problem in HetIoT, i.e., the devices in different network types suffer interference with each other because of their co-existence.

2.2. Performance modeling of guard-zone based HetIoT

Establishing guard zones is a widely adopted strategy to mitigate interference across various network types, including ad hoc networks [26, 27], UAV networks [28], and D2D-enabled HetIoT [16]. Some related work , guard zones are generally positioned around both cellular and D2D devices, as discussed below. Establishing guard zones is a widely adopted strategy to mitigate interference across various network types, including ad hoc networks [26, 27], UAV networks [28], and D2D-enabled HetIoT [16]. Some studies explored the use of guard zones in HetIoT. For instance, [29] develops a stochastic geometry-based theoretical model study the STPs for both cellular and D2D devices in D2D underlaid cellular network. In this network, guard zones are implemented centered around BSs to mitigate the interference. Within these zones, D2D devices are required to operate in cellular mode; outside the zones, they operate in D2D mode. In [20], they investigate a D2D and cellular coexisting network, where D2D devices outside the guard zones around BSs are active, while cellular devices are divided into "central" users within the guard zones and "edge" users outside them. Utilizing stochastic geometry, their model characterize the location randomness of various types devices. Similarly, Chen et al. in [30] combine SIR-aware link activation with guard zones around BSs to evaluate the impact of guard zone radius and SIR threshold on D2D throughput and cellular coverage. Shi et al. in [31] set exclusion regions around cellular users in D2D-aided uplink cellular networks and analyze the coverage probabilities for both cellular and D2D devices using a stochastic geometry approach. Beyond guard zones around BSs, other works, such as [17, 32], establish guard zones around D2D transmitters, primarily aiming to reduce interference from cellular transmissions.

In summary, the majority of previous studies focus on setting guard zones around BSs to reduce interference from transmitting BSs on other network components, they often overlook the impact of transmitting cellular devices on D2D communications. In a dense HetIoT network, cellular and D2D devices closely coexist, the interference generated by transmitting cellular devices can significantly affect D2D transmission performance. In comparison, our work considers two distinct types of guard zones around both BSs and cellular devices to ensure sufficient spatial separation between cellular and D2D transmissions.

3. System Model

3.1. Network deployment

Fig. 2 illustrates a guard-zone-based HetIoT comprising base stations (BSs), cellular devices, and D2D devices. The BSs, cellular devices, and D2D devices are assumed to be randomly distributed according to three independent homogeneous Poisson point processes (HPPPs). Φ_b, Φ_c, Φ_d with densities λ_b, λ_c, λ_d ($\lambda_c \gg \lambda_b$, $\lambda_d \gg \lambda_b$), respectively. Each cellular device is associated with its geographically nearest BS, thereby a whole cellular network forms a topology of a Voronoi tessellation, as shown in Fig. 2(a). Let S_v be the area of a Voronoi cell, then $\mathbb{E}\left[S_v\right] = 1/\lambda_b$ [19]. Each Voronoi cell is approximated as a circle with radius R_v [33], then $R_v = \sqrt{\mathbb{E}\left[S_v\right]/\pi} = \sqrt{1/\pi\lambda_b}$. In HetIoT, the BSs, cellular devices and D2D devices transmit data with a fixed transmission power P_b, P_c and P_d, respectively.

Considering the spectrum limit, all cellular transmissions and D2D transmissions among the three devices share the same band, then causing interference with each other. In particular, cellular transmissions between BSs and cellular devices, including both downlink (from BS to cellular device) and uplink (from cellular device to BS) transmissions, are performed in a Voronoi cell. Given one carrier in a Voronoi cell, only a downlink or uplink transmission can in use at the same time. As in Fig. 2(a) shows, the cellular devices in the Voronoi cell of a BS under transmission cannot initiate a new transmission via the same carrier; in contrast, the cellular devices in a Voronoi cell can transmit data to the BS when it is not under transmission. For D2D transmissions, we assume that a D2D device may choose to operate in either HD or FD mode with a maximum transmission distance d_d. Since the cellular and D2D transmissions may interfere with each other, guard zones at the sides of transmitting BSs and cellular devices are set. In the guard zone centered at each transmitting BS with radius d_b or in the guard zone centered at each transmitting cellular device with radius d_c, the D2D devices cannot be activated to perform any transmission. As Fig. 2(a) shows, D2D devices in the guard zones of transmitting BSs or cellular devices are non-activated; in contrast, D2D devices outside the guard zones are activated. The main notations used in this paper and their descriptions are summarized in Table 1.

Table 1
Key notations and their descriptions.

Notations	Descriptions of BSs' Parameters
Φ_b, λ_b	HPPP of BSs with density λ_b
Φ_b^t, λ_b^t	HPPP of transmitting BSs with density λ_b^t
p_b^t	Transmission probability of each BS
d_b	Radius of BS's guard zone
R_b	Distance between BS and cellular device with PDF $f_{R_b}(r_b)$
I_b^*	Interference at BS from transmitting devices
Notations	**Descriptions of cellular devices' Parameters**
Φ_c, λ_c	HPPP of cellular devices with density λ_c
Φ_c^t, λ_c^t	Point process of transmitting cellular devices with λ_c^t
$\widetilde{\Phi}_c^t$	Approximated HPPP of activated cellular devices
p_t	Probability that cellular device accesses the channel
p_c^t	Transmission probability of each cellular device
d_c	Radius of cellular device's guard zone
R_c	Distance from cellular device to BS with PDF $f_{R_c}(r_c)$
I_c^*	Interference at cellular device from transmitting devices
Notations	**Descriptions of D2D devices' Parameters**
Φ_d, λ_d	HPPP of D2D devices with density λ_d
Φ_d^a, λ_d^a	Point process of activated D2D devices with density λ_d^a
$\widetilde{\Phi}_d^a$	Approximated HPPP of activated D2D devices
Φ_H, λ_H	HPPP of activated HD D2D devices with density λ_H
Φ_F, λ_F	HPPP of activated FD D2D devices with density λ_F
Φ_H^t, λ_H^t	HPPP of transmitting HD D2D devices with density λ_H^t
Φ_F^t, λ_F^t	HPPP of transmitting FD D2D devices with density λ_F^t
$\mathbb{P}_b/\mathbb{P}_c$	Probability that a D2D device locates outside the guard zones of transmitting BSs/CUs
p_a	Probability that a D2D device is activated
p_H/p_F	Probability that a D2D device operates in HD/FD mode
d_d	Maximum transmission distance of each D2D device
R_d	Distance between two D2D devices with PDF $f_{R_d}(r_d)$
κ	Self-interference cancellation factor
I_d^*	Interference at D2D device from transmitting devices
Notations	**Descriptions of Public Parameters**
$\mathbb{E}[S_v]$	Mean area of each Voronoi cell S_v
R_v	Approximated radius of circular Voronoi cell
p_d/p_u	Probability of DL/UL transmission in a cell
θ/θ_{dB}	SINR threshold (unitless/dB)
H	Channel power fading coefficient
α	Path-loss exponent
σ^2	Additive white Gaussian noise with variance σ^2
$*$	$* \in \{b, c, d\}$ denotes BS, cellular device, D2D device, respectively
$SINR_*$	Received SINR at $*$
S_*	*'s received signal power
P_*	Transmission power of each *
$\mathcal{P}_*$	Successful transmission probability of *

3.2. Channel model

Without loss of generality, all the wireless signals in cellular and D2D transmissions undergo both large-scale and small-scale channel fading. The former is characterized by

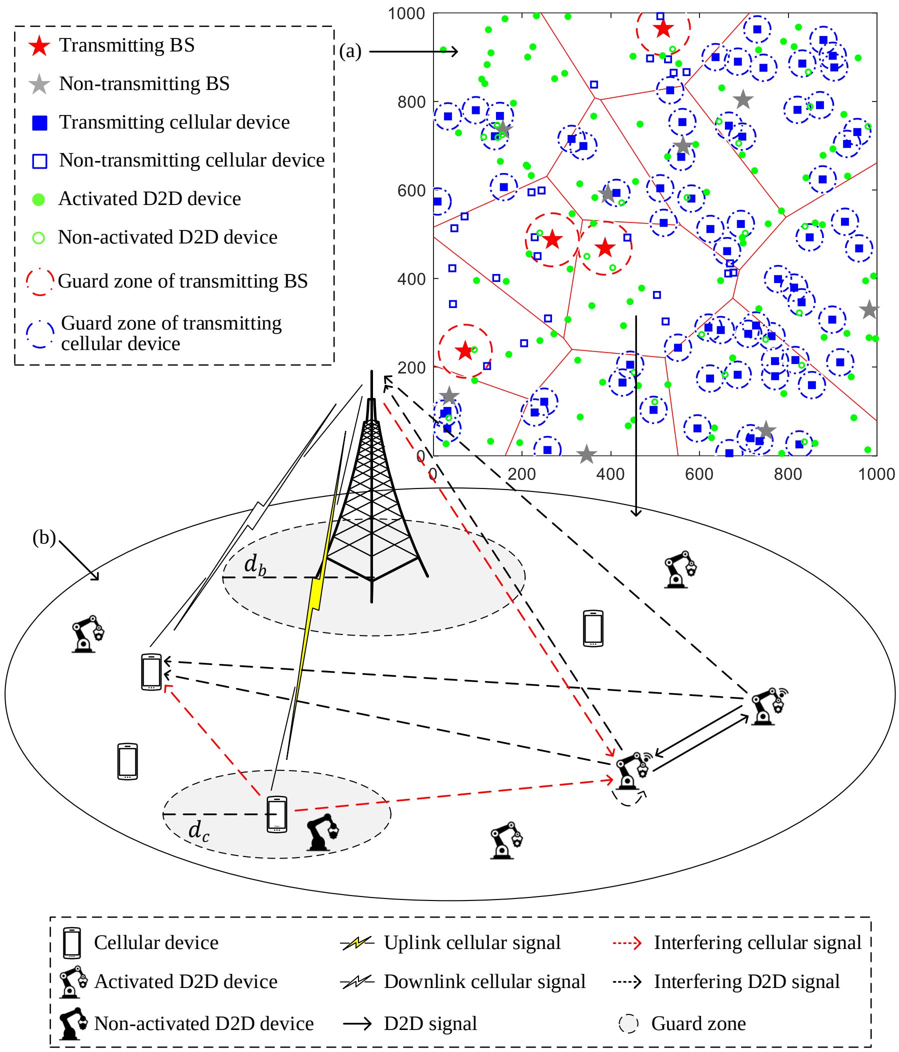

Figure 2: (a) A snapshot of Voronoi tessellation of BSs, cellular devices and D2D devices in a 1000*1000 m square region, where $\lambda_b = 10$ BSs km^{-2}, $\lambda_c = 100$ cellular devices km^{-2}, $\lambda_d = 100$ D2D devices km^{-2}, $d_b = 60$ m, $d_c = 30$ m, $p_d = 0.5$, $p_t = 1.0$. (b) A cell of a guard-zone based HetIoT.

the distance-dependent power-law path loss model in which the signal power decays at the rate $R^{-\alpha}$ [34], where R is Euclidean distance between a transmitter and a receiver, and α is the path-loss exponent which usually satisfies $2 < \alpha < 6$ [35]. The latter is modeled by an independent and identically distributed (i.i.d.) channel power gain H, which follows exponential distribution with mean $1/\mu$, i.e., $H \sim \exp(\mu)$ [36, 37]. Besides, the noise at the receiver is modeled as an additive white Gaussian variable with zero mean and variance σ^2 [38, 39].

3.3. Density of transmitting cellular devices

Recall that both downlink and uplink cellular transmissions are performed in a Voronoi cell. In all cellular transmissions of HetIoT, let p_d and p_u be the distribution ratio of downlink and uplink transmissions, respectively. Then $p_d + p_u = 1$. The transmission probability of a BS can be given by the downlink transmission ratio $p_b^t = p_d$. Accordingly, we can apply the thinning operation to the BS distribution Φ_b and generate a new distribution Φ_b^t with density λ_b^t for all BSs under transmissions (we called it transmitting BSs). The value of λ_b^t is given by $\lambda_b^t = p_b^t \lambda_b$ [18, 19]. For the uplink transmissions, all cellular devices adopt ALOHA mechanism to access the channel with probability p_t [14]. Hence, the transmission probability of each cellular device $p_c^t = p_u p_t$. After excluding the cellular devices in the Voronoi cell of each transmitting BS and the cellular devices that do not attempt to transmit data, the remained transmitting cellular devices form a general point process Φ_c^t with density λ_c^t. The density of transmitting cellular devices λ_c^t can be given by $\lambda_c^t = p_c^t \lambda_c^u$.

3.4. Density of transmitting D2D devices

In D2D transmissions, a D2D device can be activated under two necessary conditions:

- **C1**: A D2D device is located outside the guard zones of transmitting BSs, the probability of which is denoted by $\mathbb{P}_b$; and
- **C2**: A D2D device is located outside the guard zones of transmitting cellular devices, the probability of which is denoted by $\mathbb{P}_c$.

The conditions **C1** and **C1** are independent of each other. Let p_a be the activated probability of a D2D device, which is given by

$$p_a = \mathbb{P}\left(\mathbf{C1}, \mathbf{C2}\right) = \mathbb{P}(\mathbf{C1})\mathbb{P}(\mathbf{C2}) = \mathbb{P}_b\mathbb{P}_c. \tag{1}$$

Next we need to calculate $\mathbb{P}_b$ and $\mathbb{P}_c$, respectively.

Given the distributions of transmitting BSs Φ_b^t and and the D2D devices Φ_d, the D2D devices outside the guard zones (i.e., holes) centered at transmitting BSs with radius d_b form a Poisson hole process (PHP) Φ_d^b [18, 19]. In Φ_d^b, the activated probability a D2D device $\mathbb{P}_b$ is given by

$$\mathbb{P}_b = \exp\left(-\lambda_b^t \pi d_b^2\right). \tag{2}$$

We use an HPPP $\widetilde{\Phi}_c^t$ with the density λ_c^t to approximate the general point process Φ_c^t of transmitting cellular devices[1]. Given the distributions of transmitting cellular devices $\widetilde{\Phi}_c^t$ and D2D devices Φ_d, the D2D devices outside the guard zones (i.e., holes) centered at transmitting cellular devices with radius d_c form another PHP Φ_d^c. In Φ_d^c, the activated probability a D2D device $\mathbb{P}_c$ is given by

$$\mathbb{P}_c = \exp\left(-\lambda_c^t \pi d_c^2\right). \tag{3}$$

Substituting (22) and (11) into (4), we have

$$p_a = \mathbb{P}_b\mathbb{P}_c = \exp\left(-\pi\left(\lambda_b^t d_b^2 + \lambda_c^u d_c^2\right)\right). \tag{4}$$

According to (4), we can see that the activated D2D devices form a point process Φ_d^a with density λ_d^a given by $\lambda_d^a = p_a\lambda_d$. A D2D device is assumed to operate in HD and FD with probability p_H and p_F, respectively, where $p_H + p_F = 1$. Let an HPPP $\widetilde{\Phi}_d^a$ with the density λ_d^a approximate the general point process Φ_d^a of activated D2D devices [40]. $\widetilde{\Phi}_d^a$ is the union of two independent PPPs Φ_H of activated HD D2D devices with density λ_H and Φ_F of activated FD D2D devices with density λ_F [14]. Then we have

$$\begin{aligned} &\widetilde{\Phi}_d^a = \Phi_H \cup \Phi_F, \\ &\lambda_H = p_H \cdot \lambda_d^a, \lambda_F = p_F \cdot \lambda_d^a. \end{aligned} \tag{5}$$

We consider a general case in D2D transmissions, i.e., half of the HD D2D devices are transmitters and half of them are receivers [14]. The transmitting HD D2D devices form an HPPP Φ_H^t with density λ_H^t, where $\lambda_H^t = \lambda_H/2$. For FD mode D2D devices, all users are transceivers at the same time. The transmitting FD D2D devices form an HPPP Φ_F^t with density λ_F^t, where $\lambda_F^t = \lambda_F$.

[1]The approximation can be found in many existing works [40]. The approximated PPP is inhomogeneous with constant positive density.

4. Analytical Model

This section develops a stochastic geometry-based analytical model to derive the expressions of STPs for the BSs, cellular and D2D transmissions.

We first introduce a general expression of the STP. Consider a wireless transmission signal from a tagged transmitter x to a tagged receiver y within a distance R_x, where the location distribution of x follows the point process Φ, and $R_x \in [0, \hat{R}_x]$. Let P_x and H_x denote the transmission power of x and the channel power gain between x and y, respectively. Let SINR_y denote the signal-to-interference-plus-noise ratio (SINR) between y received x's signal power S_y and its suffered interference signal power I_y plus noise power σ^2. The value of SINR_y can be given by [41, 42]

$$\mathrm{SINR}_y\left(R_x, I_y\right) = \frac{S_y}{I_y + \sigma^2} = \frac{P_x H_x R_x^{-\alpha}}{I_y + \sigma^2}. \tag{6}$$

In (6), $I_y = \sum_{x'\in\Phi'} P_{x'} H_{x'} R_{x'}^{-\alpha}$, where $x' \in \Phi'$ is the interfering transmitter with set Φ', $P_{x'}$ denotes the transmission power of x', $H_{x'}$ and $R_{x'}$ are the channel power gain and the transmission distance between x' and y, respectively.

For the tagged receiver y, the signal from x can be successfully received and decoded only when SINR_y (Unitless) at y exceeds a certain SINR threshold θ_{dB} (in decibel (dB)) [2]. Let $\mathbb{P}_x$ denote the conditional success probability (CSP) of x's transmission, which is given by

$$\mathbb{P}_x = \mathbb{P}\left(\mathrm{SINR}_y\left(R_x, I_y\right) > \theta \middle| \Phi\right). \tag{7}$$

Let $\mathcal{P}_x$ denote the STP of x. The overall network performance can be defined as the mean value of $\mathbb{P}_x$, i.e.,

$$\begin{aligned} \mathcal{P}_x &= \mathbb{E}_\Phi\left[\mathbb{P}_x \middle| \Phi\right] \\ &= \mathbb{E}_{R_x, I_y}\left[\mathbb{P}\left(\mathrm{SINR}_y\left(R_x, I_y\right) > \theta\right) \middle| \Phi\right] \\ &= \int_0^{\hat{R}_x} \mathbb{P}\left(\mathrm{SINR}_y\left(r_x, I_y\right) > \theta \middle| \Phi\right) \cdot f_{R_x}\left(r_x\right) \mathrm{d}r_x, \end{aligned} \tag{8}$$

where $f_{R_x}\left(r_x\right)$ is the probability density function (PDF) of R_x. In (8), $\mathbb{P}\left(\mathrm{SINR}_y\left(r_x, I_y\right) > \theta \middle| \Phi\right)$ can be further calculated as follows.

$$\begin{aligned} &\mathbb{P}\left(\mathrm{SINR}_y\left(r_x, I_y\right) > \theta \middle| \Phi\right) = \mathbb{P}\left(\frac{P_x H_x r_x^{-\alpha}}{I_y + \sigma^2} > \theta \middle| \Phi\right) \\ &= \mathbb{P}\left(H_x > \frac{\theta r_x^\alpha}{P_x}\left(I_y + \sigma^2\right) \middle| \Phi\right) \\ &\overset{(a)}{=} \mathbb{E}_{I_y}\left[\exp\left(\frac{\mu\theta r_x^\alpha}{P_x}\left(I_y + \sigma^2\right)\right)\right] \\ &= \exp(-s\sigma^2)\mathbb{E}_{I_y}\left[\exp(-sI_y)\right] \\ &\overset{(b)}{=} \exp(-s\sigma^2)\mathcal{L}_{I_y}(s), \end{aligned} \tag{9}$$

[2]The real ratio value of θ_{dB} is given by $\theta = 10^{\theta_{dB}/10}$ (Unitless).

where $s = \mu\theta r_x^\alpha / P_x$, $\mathbb{E}_X[f(X)]$ is the expectation of $f(X)$ with respect to X. (a) is resulted from the exponential distribution of H_x with mean $1/\mu$ [3], i.e., $H_x \sim \exp(\mu)$. According to the cumulative distribution function of an exponential distribution, if $f_{H_x}(h_x) = \mu e^{-\mu h_x}$, $P(H_x > h_0) = 1 - F_{H_x}(h_0) = 1 - P(H_x \le h_0) = 1 - \int_0^{h_0} \mu e^{-\mu h_x} dh_x = \exp(-\mu h_0)$. (b) comes from the definition of Laplace transform (LT) of interference I_y, evaluated at s, that is $\mathcal{L}_{I_y}(s) = \mathbb{E}[\exp(-sI_y)]$.

Based on the general expression of STP, we can express the STPs of BSs, cellular devices and D2D devices in sequence.

4.1. STP of BSs $\mathcal{P}_b$

In a Voronoi cell, a tagged BS b_0 performs the downlink transmission to a tagged cellular device c_0. When c_0 receives the desired signal from b_0, it also suffers from the interference of the other transmitting BSs, cellular devices, D2D devices in HD/FD mode. Let $\mathrm{SINR}_c(R_b, I_c)$ denote the SINR at the cellular device c_0. The value of $\mathrm{SINR}_c(R_b, I_c)$ is given by

$$\mathrm{SINR}_c(R_b, I_c) = \frac{S_c}{I_c + \sigma^2} = \frac{P_b H_b R_b^{-\alpha}}{I_c^b + I_c^c + I_c^H + I_c^F + \sigma^2}, \tag{10}$$

where S_c, I_c and σ^2 are the desired signal power, aggregate interference power and noise power at c_0, respectively. P_b is the transmission power of BS, H_b and R_b are the channel power gain and transmission distance between b_0 and c_0, respectively. The terms $I_c^b, I_c^c, I_c^H, I_c^F$ are interferences caused by the other transmitting BSs, cellular devices, D2D devices in HD/FD mode at c_0, respectively. Their values are given as follow.

$$I_c^b = \sum_{i \in \Phi_b^t / \{b_0\}} P_b H_i R_i^{-\alpha}, I_c^c = \sum_{i \in \Phi_c^t} P_c H_i R_i^{-\alpha},$$
$$I_c^H = \sum_{i \in \Phi_H^t} P_d H_i R_i^{-\alpha}, I_c^F = \sum_{i \in \Phi_F^t} P_d H_i R_i^{-\alpha}.$$

Let $\mathcal{P}_b$ denote the STP of BSs. Based on Eq. (7)-(9), $\mathcal{P}_b$ can be calculated by

$$\begin{aligned}\mathcal{P}_b &= \mathbb{E}_{R_b, I_c}\left[\mathbb{P}\left(\mathrm{SINR}_c(R_b, I_c) > \theta\right) \middle| \Phi\right] \\ &= \int_0^{R_v} \mathbb{E}_{I_c}\left[\mathbb{P}\left(\mathrm{SINR}_c(r_b, I_c) > \theta\right)\right] \cdot f_{R_b}(r_b)\, \mathrm{d}r_b,\end{aligned} \tag{11}$$

where $f_{R_b}(r_b)$ is PDF of R_b, $R_b \in [0, R_v]$ and R_v is the approximated radius of circular Voronoi cell. In Eq. (11), $f_{R_b}(r_b)$ can be calculated by [43]

$$\begin{aligned} f_{R_b}(r_b) &= \mathrm{d}\frac{F_{R_b}(r_b)}{\mathrm{d}r_b} = \mathrm{d}\frac{\mathbb{P}(R_b \le r_b)}{\mathrm{d}r_b} \\ &= \mathrm{d}\frac{r_b^2 / R_v^2}{\mathrm{d}r_b} = 2r_b / R_v^2 = 2\pi\lambda_b r_b. \end{aligned}$$

[3] In our simulation, we set $\mu = 1$, i.e., $\mu \sim \exp(1)$.

where $F_{R_b}(r_b) = \mathbb{P}(R_b \le r_b)$ is the cumulative distribution function of R_b [44, 45]. In Eq. (11), we can calculate $\mathbb{E}_{I_c}\left[\mathbb{P}\left(\mathrm{SINR}_c(r_b, I_c) > \theta\right)\right]$ as

$$\begin{aligned} &\mathbb{E}_{I_c}\left[\mathbb{P}\left(\mathrm{SINR}_c(r_b, I_c) > \theta\right)\right] \\ &= \mathbb{E}_{I_c^b, I_c^c, I_c^H, I_c^F}\left[\exp\left(-\frac{\mu\theta r_b^\alpha}{P_b}\left(I_c^b + I_c^c + I_c^H + I_c^F + \sigma^2\right)\right)\right] \\ &= \exp\left(-s_c\sigma^2\right)\mathcal{L}_{I_c^b}(s_c)\,\mathcal{L}_{I_c^c}(s_c)\,\mathcal{L}_{I_c^H}(s_c)\,\mathcal{L}_{I_c^F}(s_c), \end{aligned} \tag{12}$$

where $s_c = \frac{\mu\theta r_b^\alpha}{P_b}$. The terms $\mathcal{L}_{I_c^b}(s_c)$, $\mathcal{L}_{I_c^c}(s_c)$, $\mathcal{L}_{I_c^H}(s_c)$, and $\mathcal{L}_{I_c^F}(s_c)$, are LTs of I_c^b, c_b^c, c_b^H, and c_b^F evaluated at s_c, respectively. We derive their expressions below.

First, the LT of I_c^b at c_0 is given by

$$\mathcal{L}_{I_c^b}(s_c) = \exp\left(-2\pi\lambda_b^t r_b^2 \theta^{2/\alpha} \int_{\frac{R_v}{r_b \theta^{1/\alpha}}}^{\infty} \frac{y}{1 + y^\alpha} dy\right). \tag{13}$$

Proof:

$$\begin{aligned} \mathcal{L}_{I_c^b}(s_c) &= \mathbb{E}_{I_c^b}\left[\exp\left(-s_c I_c^b\right)\right] \\ &= \mathbb{E}_{R_i, H_i}\left[\exp\left(-\frac{\mu\theta r_b^\alpha}{P_b}\sum_{i \in \Phi_b^t / \{b_0\}} P_b H_i R_i^{-\alpha}\right)\right] \\ &\overset{(a)}{=} \mathbb{E}_{R_i}\left[\mathbb{E}_{H_i}\left[\exp\left(-\sum_{i \in \Phi_b^t / \{b_0\}} \mu\theta r_b^\alpha H_i R_i^{-\alpha}\right)\right]\right] \\ &\overset{(b)}{=} \mathbb{E}_{R_i}\left[\prod_{i \in \Phi_b^t / \{b_0\}} \mathbb{E}_{H_i}\left(\exp\left(-\mu\theta r_b^\alpha R_i^{-\alpha} H_i\right)\right)\right] \\ &\overset{(c)}{=} \mathbb{E}_{R_i}\left[\prod_{i \in \Phi_b^t / \{b_0\}} \int_0^\infty \exp\left[-\mu\theta r_b^\alpha R_i^{-\alpha} h_i\right] f_{H_i}(h_i)\, \mathrm{d}h_i\right] \\ &\overset{(d)}{=} \mathbb{E}_{R_i}\left[\prod_{i \in \Phi_b^t / \{b_0\}} \int_0^\infty \exp\left[-\mu\theta r_b^\alpha R_i^{-\alpha} h_i\right] \mu \exp\left(-\mu h_i\right) \mathrm{d}h_i\right] \\ &= \mathbb{E}_{R_i}\left[\prod_{i \in \Phi_b^t / \{b_0\}} \left(\frac{\mu}{\mu + \mu\theta r_b^\alpha R_i^{-\alpha}}\right)\right] \end{aligned} \tag{14}$$

In Eq. (14), (a) comes from the fact that R_i and H_i are mutually independent. (b) results from the property of exponential distribution, i.e., $\exp\left(\sum_i H_i\right) = \prod_i \exp\left(H_i\right)$. (c) is due to the definition of expectation of H_i. (d) holds because H_i follows an exponential distribution with mean $1/\mu$, i.e., $f_{H_i}(h_i) = \mu e^{-\mu h_i}$. According to the probability generation functional (PGFL) of an HPPP Φ with density λ, i.e., $\mathbb{E}\left[\prod_{x \in \Phi} f(x)\right] = \exp\left(-\lambda \int_{\mathbb{R}^d} (1 - f(x))\, \mathrm{d}x\right)$, we have

$$
\begin{aligned}
&\mathcal{L}_{I_c^b}\left(s_c\right) \\
&\overset{(a)}{=} \exp\left(-\lambda_b^t \int_{\mathbb{R}^2/\mathcal{B}(c_0,R_v)} \left(1-\frac{1}{1+\theta r_b^{\alpha} r_i^{-\alpha}}\right) \mathrm{d}r_i\right) \\
&\overset{(b)}{=} \exp\left(-\lambda_b^t \int_0^{2\pi} \int_{R_v}^{\infty} \left(\frac{\theta r_b^{\alpha} r_i^{-\alpha}}{1+\theta r_b^{\alpha} r_i^{-\alpha}}\right) r_i \mathrm{d}r_i \mathrm{d}\alpha\right) \\
&= \exp\left[-2\pi\lambda_b^t \int_{R_v}^{\infty} \frac{1}{1+\frac{1}{\theta r_b^{\alpha} r_i^{-\alpha}}} r_i \mathrm{d}r_i\right] \qquad (15)\\
&\overset{(c)}{=} \exp\left[-2\pi\lambda_b^t \int_{\frac{R_v}{r_b\theta^{1/\alpha}}}^{\infty} \left(\frac{1}{1+y^{\alpha}}\right) y r_b^2 \theta^{2/\alpha} \mathrm{d}y\right] \\
&= \exp\left[-2\pi\lambda_b^t r_b^2 \theta^{2/\alpha} \int_{\frac{R_v}{r_b\theta^{1/\alpha}}}^{\infty} \frac{y}{1+y^{\alpha}} \mathrm{d}y\right].
\end{aligned}
$$

In Eq. (15)(a), $R^2/\mathcal{B}\left(c_0, R_v\right)$ is the area in which the interfering BSs locate, which excludes the current Voronoi cell that the origin receiving tagged cellular device c_0 locates, $\mathcal{B}\left(c_0, R_v\right)$ is a circular region centered at the origin c_0 with radius R_v. (b) converts the expression from orthogonal coordinates to polar coordinates, where α is the polar angle which is uniformly distributed in $[0,\ 2\pi]$; in Eq. (f), the integration limits are from R_v to ∞ since the closest interfering BS is at least at a distance R_v. (c) follows by changing the variable $y^{\alpha} = \frac{1}{\theta r_b^{\alpha} r_i^{-\alpha}}$, i.e, $y = \frac{r_i}{r_b\theta^{1/\alpha}}$, hence y belongs to $\left(\frac{R_v}{r_b\theta^{1/\alpha}}, \infty\right)$.

For the special case $\alpha = 4$, we have

$$
\begin{aligned}
\mathcal{L}_{I_c^b}\left(s_c\right) &= \exp\left[-2\pi\lambda_b^t r_b^2 \sqrt{\theta} \int_{\frac{R}{r_b\theta^{1/4}}}^{\infty} \frac{y}{1+y^4} \mathrm{d}y\right] \\
&\overset{(a)}{=} \exp\left[-\pi\lambda_b^t r_b^2 \sqrt{\theta} \cdot \left(\frac{\pi}{2} - \tan^{-1}\left(\frac{R^2}{r_b^2\sqrt{\theta}}\right)\right)\right],
\end{aligned} \qquad (16)
$$

where (a) follows $\int_A^{\infty} \frac{x}{1+x^{\alpha}} \mathrm{d}x = \frac{1}{4}\left(\pi - 2\tan^{-1}\left(A^2\right)\right)$. ■

In (12), the LT of I_c^c at c_0 is given as

$$
\mathcal{L}_{I_c^c}\left(s_c\right) = \exp\left(-\lambda_b^t \left(s_c P_c\right)^{2/\alpha} \cdot \frac{2\pi^2}{\alpha\sin\left(2\pi/\alpha\right)}\right) \qquad (17)
$$

Proof:

$$
\begin{aligned}
\mathcal{L}_{I_c^b}\left(s_c\right) &= \mathbb{E}_{I_c^b}\left[\exp\left(-s_c I_c^b\right)\right] \\
&= \mathbb{E}_{R_i,H_i}\left[\exp\left(-s_c \sum_{i\in\Phi_b^t/\{b_0\}} P_c H_i R_i^{-\alpha}\right)\right] \\
&= \mathbb{E}_{R_i}\left[\mathbb{E}_{H_i}\left[\exp\left(-\sum_{i\in\Phi_b^t/\{b_0\}} s_c P_c H_i R_i^{-\alpha}\right)\right]\right] \\
&\overset{(a)}{=} \exp\left(-\lambda_c^t \int_{\mathbb{R}^2} \left(1-\frac{1}{1+s_c P_c r_i^{-\alpha}}\right) \mathrm{d}r_i\right) \qquad (18)\\
&\overset{(b)}{=} \exp\left(-\lambda_c^t \int_0^{2\pi} \int_0^{\infty} \left(\frac{s_c P_c r_i^{-\alpha}}{1+s_c P_c r_i^{-\alpha}}\right) r_i \mathrm{d}r_i \mathrm{d}\alpha\right) \\
&= \exp\left(-2\pi\lambda_c^t \left(s_c P_c\right)^{2/\alpha} \int_0^{\infty} \frac{y}{1+y^{\alpha}} \mathrm{d}y\right) \\
&\overset{(c)}{=} \exp\left(-\pi\lambda_c^t \left(s_c P_c\right)^{2/\alpha} \cdot \frac{2}{\alpha} \cdot \Gamma\left(\frac{2}{\alpha}\right) \cdot \Gamma\left(1-\frac{2}{\alpha}\right)\right) \\
&\overset{(d)}{=} \exp\left(-\lambda_c^t \left(s_c P_c\right)^{2/\alpha} \cdot \frac{2\pi^2}{\alpha\sin\left(2\pi/\alpha\right)}\right)
\end{aligned}
$$

In the above proof, (a) follows from the probability generation functional (PGFL) of HPPP; in (a), R^2 is the area in which the interfering cellular devices locate. (b) converts the expression from orthogonal coordinates to polar coordinates, where α is the polar angle which is uniformly distributed in $[0,\ 2\pi]$. (c) can refer to Eq. 3.241.4 in [46]. (d) follows from the Euler's reflection formula $\Gamma(x)\cdot\Gamma(1-x) = \frac{\pi}{\sin(\pi x)}$ where $\Gamma(x)$ is the complete gamma function $\Gamma(x) = \int_0^{\infty} t^{x-1} e^{-t} \mathrm{d}t$. ■

Following the similar derivation process in $\mathcal{L}_{I_c^c}$, the LT of I_c^H and I_c^F at c_0 are given as follows.

$$
\mathcal{L}_{I_c^H}\left(s_c\right) = \exp\left(-\lambda_H^t \left(s_c P_d\right)^{2/\alpha} \cdot \frac{2\pi^2}{\alpha\sin\left(2\pi/\alpha\right)}\right), \qquad (19)
$$

$$
\mathcal{L}_{I_c^F}\left(s_c\right) = \exp\left(-\lambda_F^t \left(s_c P_d\right)^{2/\alpha} \cdot \frac{2\pi^2}{\alpha\sin\left(2\pi/\alpha\right)}\right). \qquad (20)
$$

4.2. STP of a cellular device $\mathcal{P}_c$

In a Voronoi cell, a tagged cellular device c_0' can perform the uplink transmission to a tagged BS b_0'. When b_0' receives the desired signal from c_0', it also suffers from the interference cause by the other transmitting BSs, cellular devices, D2D devices in HD/FD mode. Let $\mathrm{SINR}_b\left(R_c, I_b\right)$ denote the SINR at the BS b_0'. The value of $\mathrm{SINR}_b\left(R_c, I_b\right)$ is given by

$$
\mathrm{SINR}_b\left(R_c, I_b\right) = \frac{S_b}{I_b+\sigma^2} = \frac{P_c H_c R_c^{-\alpha}}{I_b^b + I_b^c + I_b^H + I_b^F + \sigma^2}, \qquad (21)
$$

where S_b, I_b and σ^2 are the desired signal power, aggregate interference power and noise power at b_0', respectively. P_c

is the transmission power of cellular device, H_c and R_c are the channel power gain and transmission distance between c_0' and b_0', respectively. Besides, $I_b^b, I_c^c, I_c^H, I_c^F$ are interference from the other transmitting BSs, cellular devices, HD D2D devices and FD D2D devices at b_0', respectively. Their values are given by

$$I_b^b = \sum_{i\in\Phi_b^t} P_b H_i R_i^{-\alpha}, I_c^c = \sum_{i\in\Phi_c^t/\left\{c_0'\right\}} P_c H_i R_i^{-\alpha},$$
$$I_c^H = \sum_{i\in\Phi_H^t} P_d H_i R_i^{-\alpha}, I_c^F = \sum_{i\in\Phi_F^t} P_d H_i R_i^{-\alpha}.$$

Let $\mathcal{P}_c$ denote the STP of cellular devices. Based on Eqs. (7)-(9), $\mathcal{P}_c$ can be calculated by

$$\begin{aligned}\mathbb{P}_c &= \mathbb{E}_{R_c,I_b}\left[\mathbb{P}\left(\mathrm{SINR}_b\left(R_c\right)>\theta\right)\Big|\Phi\right]\\ &= \int_0^{R_v}\mathbb{E}_{I_b}\left[\mathbb{P}\left(\mathrm{SINR}_b\left(r_c,I_b\right)>\theta\right)\right]\cdot f_{R_c}\left(r_c\right)\mathrm{d}r_c\end{aligned} \tag{22}$$

where $f_{R_c}\left(r_c\right)$ is PDF of R_c, and $R_c \in [0, R_v]$. Since the cellular devices in each Voronoi cell follow the same location distribution, R_c has the same PDF as R_b, i.e., $f_{R_c}\left(r_c\right) = 2\pi\lambda_b r_c$. In Eq. (22), $\mathbb{E}_{I_b}\left[\mathbb{P}\left(\mathrm{SINR}_b\left(r_c, I_b\right)>\theta\right)\right]$ can be calculated by

$$\begin{aligned}&\mathbb{E}_{I_b}\left[\mathbb{P}\left(\mathrm{SINR}_b\left(r_c,I_b\right)>\theta\right)\right]\\ &= \mathbb{E}_{I_b^b,I_b^c,I_b^H,I_b^F}\left[\mathbb{P}\left(\frac{P_cH_cR_c^{-\alpha}}{I_b^b+I_b^c+I_b^H+I_b^F+\sigma^2}>\theta\right)\right]\\ &= \exp\left(-s_b\sigma^2\right)\mathcal{L}_{I_b^b}\left(s_b\right)\mathcal{L}_{I_b^c}\left(s_b\right)\mathcal{L}_{I_b^H}\left(s_b\right)\mathcal{L}_{I_b^F}\left(s_b\right),\end{aligned} \tag{23}$$

where $s_b = \frac{\mu\theta r_c^\alpha}{P_c}$. The terms $\mathcal{L}_{I_b^b}\left(s_b\right)$, $\mathcal{L}_{I_b^c}\left(s_b\right)$, $\mathcal{L}_{I_b^H}\left(s_b\right)$, and $\mathcal{L}_{I_F}\left(s_b\right)$ are LTs of I_b^b, I_b^c, I_b^H, and I_b^F evaluated at s_b, respectively. Their values are given as follows.

$$\mathcal{L}_{I_b^b}\left(s_b\right) = \exp\left(-2\pi\lambda_b^t\left(s_bP_b\right)^{2/\alpha}\int_{\frac{R_v}{\left(s_bP_b\right)^{1/\alpha}}}^{\infty}\frac{y}{1+y^\alpha}\mathrm{d}y\right), \tag{24}$$

$$\mathcal{L}_{I_b^c}\left(s_b\right) = \exp\left(-2\pi\lambda_c^u r_c^2\theta^{2/\alpha}\int_{\frac{R_v}{r_c\theta^{1/\alpha}}}^{\infty}\frac{y}{1+y^\alpha}\mathrm{d}y\right), \tag{25}$$

$$\mathcal{L}_{I_b^H}\left(s_b\right) = \exp\left(-\lambda_H^t\left(s_bP_d\right)^{2/\alpha}\cdot\frac{2\pi^2}{\alpha\sin\left(2\pi/\alpha\right)}\right), \tag{26}$$

$$\mathcal{L}_{I_b^F}\left(s_b\right) = \exp\left(-\lambda_F^t\left(s_bP_d\right)^{2/\alpha}\cdot\frac{2\pi^2}{\alpha\sin\left(2\pi/\alpha\right)}\right). \tag{27}$$

4.3. STP of D2D device $\mathcal{P}_d$

For a D2D transmission from a tagged D2D device d_0^t to the other tagged D2D device d_0^r, the $\mathrm{SINR}_d\left(R_d, I_d\right)$ at d_0^r can be expressed as

$$\mathrm{SINR}_d\left(R_d,I_d\right) = \frac{S_d}{I_d+\sigma^2} = \frac{P_dH_dR_d^{-\alpha}}{I_d^b+I_d^c+I_d^H+I_d^F+I_d^s+\sigma^2} \tag{28}$$

where S_d, I_d and σ^2 are the desired signal power, aggregate interference power and noise power at d_0^r, respectively. P_d is the transmission power of D2D device, H_d and R_d are the channel power gain and transmission distance between d_0^t and d_0^r, respectively. Besides, $I_b^b, I_c^c, I_c^H, I_c^F$ are interferences caused by the other transmitting BSs, cellular devices, HD D2D devices and FD D2D devices at d_0^r's, respectively. Their values are given as follows.

$$I_b^b = \sum_{i\in\Phi_b^t} P_b H_i R_i^{-\alpha}, I_c^c = \sum_{i\in\Phi_c^t} P_c H_i R_i^{-\alpha},$$
$$I_c^H = \sum_{i\in\Phi_H^t/\left\{d_0^t\right\}} P_d H_i R_i^{-\alpha},$$
$$I_c^F = \sum_{i\in\Phi_F^t/\left\{d_0^t\right\}} P_d H_i R_i^{-\alpha}.$$

In addition, $I_d^s = \kappa P_d \mathbb{1}_{FD}$ is the self-interference due to the FD D2D transmission, κ is the self-interference cancellation factor, $\mathbb{1}_{FD}$ is the indicator function which takes value 1 representing D2D device operating in FD mode and 0 representing D2D device operating in HD mode.

Hence, $\mathbb{P}_d$ can be expressed as

$$\begin{aligned}\mathbb{P}_d &= \mathbb{E}_{I_d,R_d}\left[\mathbb{P}\left(\mathrm{SINR}_d\left(R_d,I_d\right)>\theta\right)\right]\\ &= \int_0^{d_d}\mathbb{E}_{I_d}\left[\mathbb{P}\left(\mathrm{SINR}_d\left(r_d,I_d\right)>\theta\right)\right]\cdot f_{R_d}\left(r_d\right)\mathrm{d}r_d\end{aligned} \tag{29}$$

where d_d is the maximum transmission distance of each D2D device, and $f_{R_d}\left(r_d\right)$ is PDF of r_d. Considering $r_d \in [0, d_d]$, $f_{R_d}\left(r_d\right) = 2r_d/d_d^2$. Then, $\mathbb{E}_{I_d}\left[\mathbb{P}\left(\mathrm{SINR}_d\left(r_d, I_d\right)>\theta\right)\right])$ can be calculated by

$$\begin{aligned}&\mathbb{E}_{I_d}\left[\mathbb{P}\left(\mathrm{SINR}_d\left(r_d,I_d\right)>\theta\right)\right]\\ &= \mathbb{E}_{I_d^b,I_d^c,I_d^H,I_d^F}\left[\mathbb{P}\left(\frac{P_dH_dr_d^{-\alpha}}{I_d^b+I_d^c+I_d^H+I_d^F+I_d^s+\sigma^2}>\theta\right)\right]\\ &= \exp\left(-s_d\sigma^2\right)\exp\left(-s_dI_d^s\right)\cdot\\ &\quad\mathcal{L}_{I_d^b}\left(s_d\right)\mathcal{L}_{I_d^c}\left(s_d\right)\mathcal{L}_{I_d^H}\left(s_d\right)\mathcal{L}_{I_d^F}\left(s_d\right),\end{aligned} \tag{30}$$

where $s_d = \frac{\mu\theta r_d^\alpha}{P_d}$. The terms $\mathcal{L}_{I_d^b}\left(s_d\right)$, $\mathcal{L}_{I_d^c}\left(s_d\right)$, $\mathcal{L}_{I_d^H}\left(s_d\right)$ and $\mathcal{L}_{I_d^F}\left(s_d\right)$ are LTs of I_d^b, I_d^c, I_d^H, and I_d^F evaluated at s_d, respectively. Their values are given as follows.

$$\mathcal{L}_{I_d^b}\left(s_d\right) = \exp\left(-2\pi\lambda_b^t\left(s_dP_b\right)^{2/\alpha}\int_{\frac{d_b}{r_0\theta_c^{1/\alpha}}}^{\infty}\frac{y}{1+y^\alpha}\mathrm{d}y\right), \tag{31}$$

Table 2
Parameters settings for simulations. Herein the notation 'x:y:z' indicates that a parameter varies from x to z in increments of y, while 'x, y' signifies that a parameter can take on the values x and y. For example, in the first row of Table 2, '-20:1:20' indicates that the parameter θ ranges from -20 dB to 20 dB in steps of 1 dB, and '4, 5' denotes that the parameter α can take the values 4 and 5, respectively.

Figure		θ(dB)	α	κ(dB)	σ^2(dBm)	d_b(m)	p_b^t	p_c^t	p_H	λ_b(/Km^2)	λ_c(/Km^2)	d_c(m)	P_d(dBm)	λ_d(/Km^2)	P_b(dBm)	P_c(dBm)
4	(a)	-20:1:20	4,5	-70	-100	50	0.5	0.5	0.5	5	50	20	1	50	23	10
	(b)	-20:1:20	4	-60, -70	-100	50	0.5	0.5	0.5	5	50	20	1	50	23	10
	(c)	-20:1:20	4	-70	-100, -50	50	0.5	0.5	0.5	5	50	20	1	50	23	10
5	(a)	5	4	-70	-100	20:20:100	0.2, 0.8	0.5	0.5	20	50	20	1	50	23	10
	(b)	5	4	-70	-100	20:20:100	0.5	0.2, 0.8	0.5	20	50	20	1	50	23	10
	(c)	5	4	-70	-100	20:20:100	0.5	0.5	0.2, 0.8	20	50	20	1	50	23	10
6	(a)	5	4	-70	-100	50	0.5	0.5	0.5	5:5:30	20, 50	20	1	50	23	10
	(b)	5	4	-70	-100	0, 50	0.5	0.5	0.5	5:5:30	50	0, 30	1	50	23	10
	(c)	5	4	-70	-100	50	0.5	0.5	0.5	5:5:30	50	20	1, 5	50	23	10

$$\mathcal{L}_{I_d^c}\left(s_d\right) = \exp\left(-2\pi\lambda_c^u\left(s_d P_c\right)^{2/\alpha}\int_{\frac{d_c}{(s_d P_c)^{1/\alpha}}}^{\infty}\frac{y}{1+y^\alpha}\mathrm{d}y\right), \tag{32}$$

$$\mathcal{L}_{I_d^H}\left(s_d\right) = \exp\left(-\lambda_H^t\left(s_d P_d\right)^{2/\alpha}\cdot\frac{2\pi^2}{\alpha\sin\left(2\pi/\alpha\right)}\right), \tag{33}$$

$$\mathcal{L}_{I_d^F}\left(s_d\right) = \exp\left(-\lambda_F^t\left(s_d P_d\right)^{2/\alpha}\cdot\frac{2\pi^2}{\alpha\sin\left(2\pi/\alpha\right)}\right). \tag{34}$$

5. Performance Evaluation

This section presents extensive Monte Carlo simulations conducted in MATLAB to validate the accuracy of the proposed theoretical model. The simulation environment is built upon the system model detailed in Section 3. Table 2 summarizes the network parameter settings in our results, which are consistent with state-of-the-art research [13, 14, 47][4].Herein P_d = 1dBm we used adapts for the practical power ranges (from 1mW to 1W) of D2D devices operating in WiFi HaLow [12]. In each simulation, the simulation region is defined as a circular disk with a radius of 10^4 m. A total of 10^4 iterations are performed for each simulation to obtain the average value. In all figures, the labels 'ana' and 'sim' represent the theoretical and simulation results, respectively.

[4]Due to page limitations, the parameter settings, such as the transmission power of BSs and cellular devices, are not comprehensively explored. In future work, one can choose suitable values for these parameter values to reflect the respective characteristics of the devices in diverse communication networks. For example, P_b=35 dBm for BSs and P_c=22 dBm for IoT devices in NB-IoT networks [10].

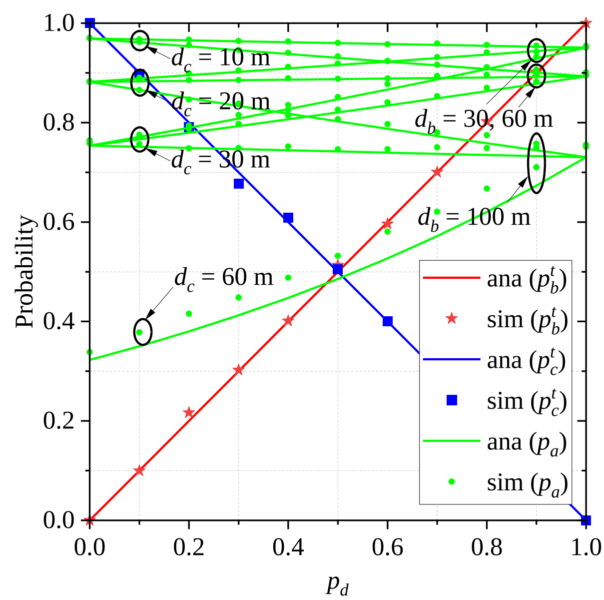

Figure 3: p_b^t, p_c^t and p_a versus p_d, where d_b= 30, 60, 100 m, d_c= 10, 20, 30, 60m.

5.1. Probabilities of transmitting BSs, transmitting cellular devices and activated D2D devices

Fig. 3 shows the variance of the probabilities of transmitting BSs p_b^t, transmitting cellular devices p_c^t and activated D2D devices p_a versus the changing values of downlink transmission probability p_d, BS guard zone's radius d_b, and cellular device guard zone's radius d_c. In the results, we have the following observations:

- As p_d increases, p_c^t decreases. This occurs because that either downlink or uplink transmission can happen in each Voronoi cell; thus, a higher p_d results in a lower p_c^t.

- For a given d_b, p_a decreases as p_d increases when d_c is small. Conversely, p_a increases as p_d increases when d_c is large. The reasoning is as follows: with a small d_c, as p_d increases, the probability of a D2D device being within the guard zone of a transmitting BS rises, increasing the likelihood that the D2D device cannot be activated, hence p_a decreases. In contrast, with a large d_c, as p_d increases, p_c^t decreases, reducing the probability of a D2D device being within the guard zone of a transmitting cellular device, which subsequently decreases the likelihood that the D2D device cannot be activated, causing p_a to increase.

- For a given d_c, p_a increases as p_d increases when d_b is small, while p_a decreases as p_d increases when d_b is large. The reasons are similar to those mentioned above.

- Given p_d and d_b, a larger d_c results in a smaller p_a. When $p_d = 1$, p_a remains constant across different values of d_c, because there are no cellular devices transmitting in any Voronoi cells. Similarly, given p_d and d_c, a larger d_b results in a smaller p_a. When $p_d = 0$, p_a remains constant across different values of d_b, because there are no BSs transmitting in any Voronoi cells.

- For small values of d_b and d_c compared to the radius R_v of each Voronoi cell, the theoretical results closely align with the corresponding simulation ones, thereby validating the accuracy of our model. However, for large values of d_b and d_c relative to R_v, the theoretical and simulation results diverge, as D2D devices are more likely to be located in the overlap areas of the guard zones of BSs and D2D devices, leading to simulation results that exceed the theoretical predictions.

5.2. STPs vs. θ

Figs. 4 shows the varieties of STPs for BSs $\mathcal{P}_b$, cellular devices $\mathcal{P}_c$, D2D devices in HD mode $\mathcal{P}_d^H$ and D2D devices in FD mode $\mathcal{P}_d^F$ versus the changing values of the SINR threshold θ, path-loss exponent α, self-interference cancellation factor κ, and noise power σ^2. In the results, we have the following observations:

- Given α, κ and σ^2, $\mathcal{P}_b$, $\mathcal{P}_c$, $\mathcal{P}_d^H$ and $\mathcal{P}_d^F$ decreases as θ increases, as shown in Figs. 4(a)-(c). This is because an increase in θ make it more difficult to decode signals from the cellular device, BS, and D2D device, respectively.

- For a fixed θ, a larger α leads to higher values of $\mathcal{P}_b$, $\mathcal{P}_c$, $\mathcal{P}_d^H$ and $\mathcal{P}_d^F$, as illustrated in Fig. 4(a). This is due to the fact that a larger α results in greater attenuation of interference signals as they propagate through space, which in turn leads to higher SINRs at the BS, cellular device and D2D device. With increased SINRs, the probabilities $\mathcal{P}_b$, $\mathcal{P}_c$, $\mathcal{P}_d^H$ and $\mathcal{P}_d^F$ also rise.

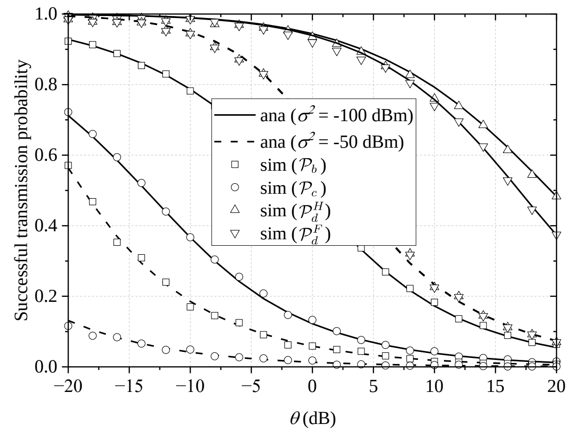

(a) α = 3, 4

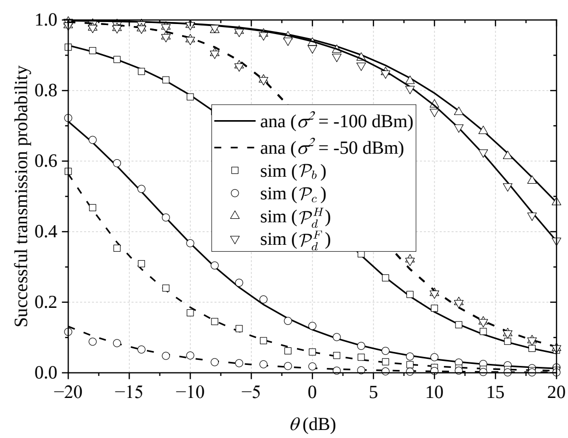

(b) κ = -60, -70 dB

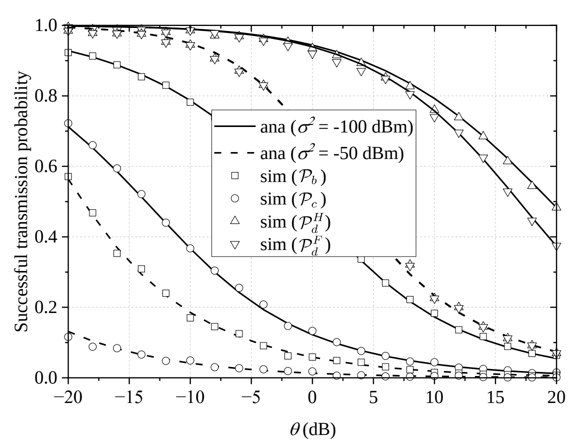

(c) σ^2 = -50, -100 dBm

Figure 4: $\mathcal{P}_b$, $\mathcal{P}_c$, $\mathcal{P}_d^H$ and $\mathcal{P}_d^F$ versus θ.

- For a fixed θ, an increase κ results in a decrease in $\mathcal{P}_d^F$, while $\mathcal{P}_d^H$, $\mathcal{P}_b$ and $\mathcal{P}_c$ remain relatively unchanged, as shown in Fig. 4(b). Note that the actual ratio value of κ (dB [14]) is expressed as $10^{\kappa/10}$ (unitless [13]). Thus, a larger κ signifies greater self-interference at the FD D2D device,leading to a decrease in its STP. However, the STPs of each BS, cellular device and HD D2D device are not significantly affected.

- For a fixed θ, an increase in σ^2 results in lower values of $\mathcal{P}_b$, $\mathcal{P}_c$, $\mathcal{P}_d^H$ and $\mathcal{P}_d^F$, as shown in Fig. 4(c). This is because that a larger σ^2 leads to lower SINRs at each BS, cellular device and HD D2D device. Consequently, With decreased SINRs, the probabilities $\mathcal{P}_b$, $\mathcal{P}_c$, $\mathcal{P}_d^H$ and $\mathcal{P}_d^F$ also decline.

5.3. STPs vs. d_b

Figs. 5 shows the varieties of STPs of BSs $\mathcal{P}_b$, cellular devices $\mathcal{P}_c$ and D2D devices in HD mode $\mathcal{P}_d^H$ and D2D devices in FD mode $\mathcal{P}_d^F$ versus the different settings of the radius of guard zone for BSs d_b, the transmission probability for BSs p_b^t, the transmission probability for cellular devices p_c^t, and the probability of HD D2D devices p_H. In the results, we have the following observations:

- Given p_b^t, p_c^t and p_H, $\mathcal{P}_d^H$ and $\mathcal{P}_d^F$ increase as d_b increases, while $\mathcal{P}_b$ and $\mathcal{P}_c$ remain relatively unchanged. This occurs because as d_b increases, the activated probability of D2D devices p_a decreases, fewer D2D transmissions lead to increased $\mathcal{P}_d^H$ and $\mathcal{P}_d^F$. In contrast, the increase of d_b does not significantly affect $\mathcal{P}_b$ and $\mathcal{P}_c$.
- Given d_b, a larger p_b^t results in lower values of $\mathcal{P}_b$, $\mathcal{P}_c$, $\mathcal{P}_d^H$ and $\mathcal{P}_d^F$, as shown in Fig. 5(a). This is because increased transmissions from BSs to cellular devices may introduce more mutual interference, negatively impacting the STPs of BSs, cellular devices and D2D devices.
- Given d_b, a larger p_c^t similarly leads to lower values of $\mathcal{P}_b$, $\mathcal{P}_c$, $\mathcal{P}_d^H$ and $\mathcal{P}_d^F$, as depicted in Fig. 5(b). The reasons for this are analogous to those discussed above.
- Given d_b, a larger p_H results in higher values of $\mathcal{P}_b$, $\mathcal{P}_c$, $\mathcal{P}_d^H$ and $\mathcal{P}_d^F$, as shown in Fig. 5(c). This occurs because increased HD D2D transmissions lead to a reduction in FD D2D transmissions, thereby decreasing the interference affecting the transmission of BSs, cellular devices and D2D devices, respectively.

5.4. STPs vs. λ_b

Figs. 6 shows the varieties of STPs of BSs $\mathcal{P}_b$, cellular devices $\mathcal{P}_c$ and D2D devices in HD mode $\mathcal{P}_d^H$ and D2D devices in FD mode $\mathcal{P}_d^F$ versus the different settings of the density of BSs λ_b, the density of cellular devices λ_c, the radius of the guard zone of cellular devices d_c and the transmission power of D2D devices P_d. In the results, we have the following observations:

- Given λ_c, d_b, d_c and P_d, $\mathcal{P}_b$ and $\mathcal{P}_c$ increase as λ_b increases, while $\mathcal{P}_d^H$ and $\mathcal{P}_d^F$ decrease. This is because an increase in λ_b reduces the area of each Voronoi cell, thus shortening the transmission distance of the desired signal between the BS and cellular device pair, leading to higher $\mathcal{P}_b$ and $\mathcal{P}_c$. Conversely, the increased density of BSs also elevates the interference power experienced by D2D devices, resulting in decrease in $\mathcal{P}_d^H$ and $\mathcal{P}_d^F$.

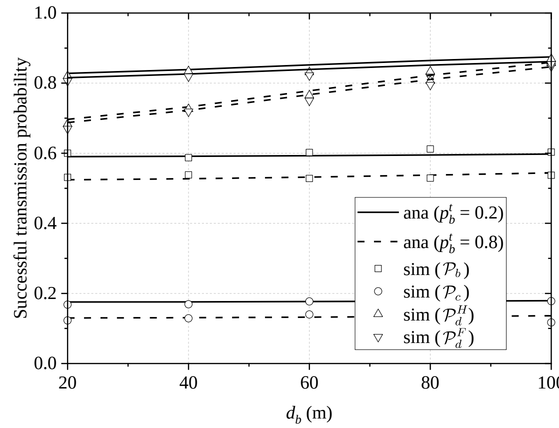

(a) p_b^t =0.2, 0.8

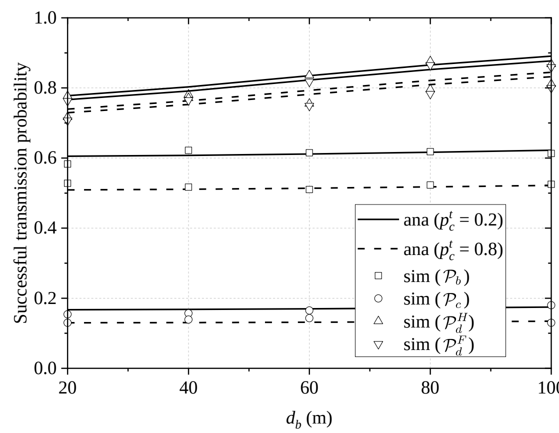

(b) p_c^t = 0.2, 0.8

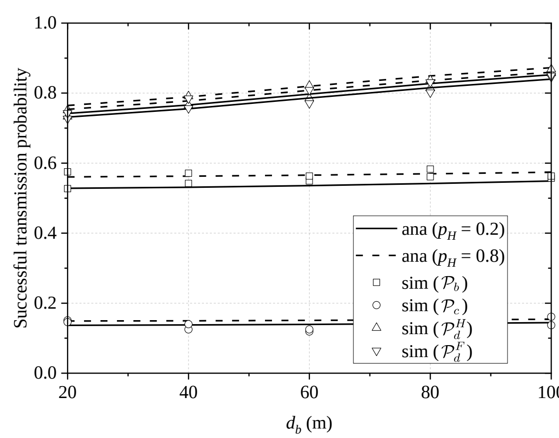

(c) p_H = 0.2, 0.8

Figure 5: $\mathcal{P}_b$, $\mathcal{P}_c$, $\mathcal{P}_d^H$ and $\mathcal{P}_d^F$ versus d_b.

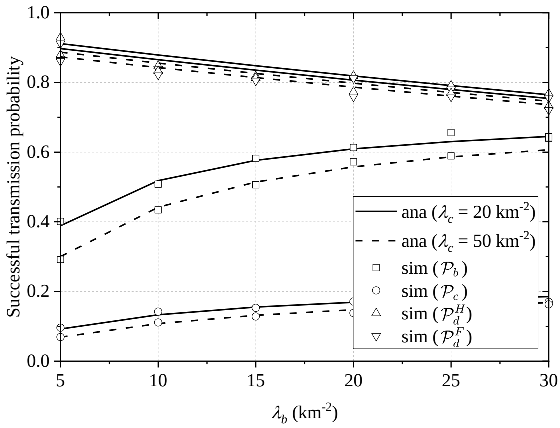

(a) $\lambda_c = 10,\ 50\ \mathrm{km}^{-2}$

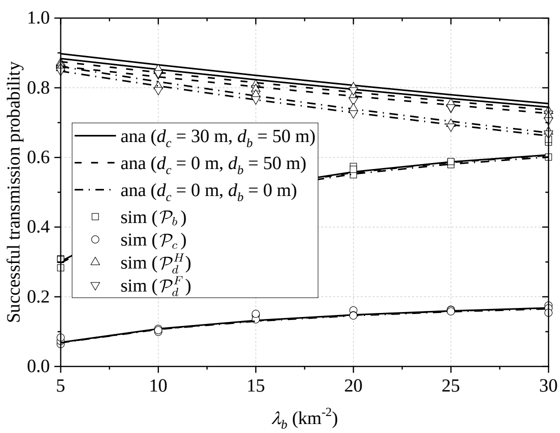

(b) $d_c = 10,\ 30$ m

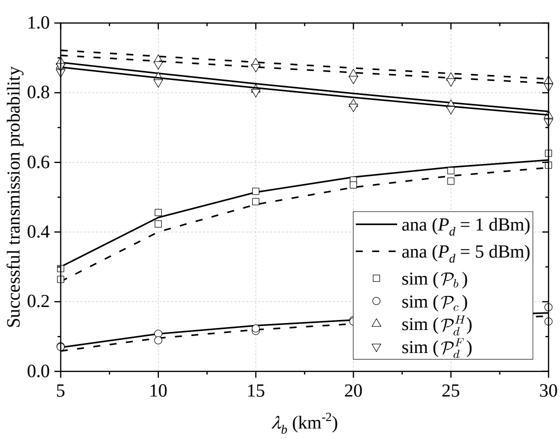

(c) $P_d = 1,\ 5$ dBm

Figure 6: $\mathcal{P}_b$, $\mathcal{P}_c$, $\mathcal{P}_d^H$ and $\mathcal{P}_d^F$ versus λ_b

- For a given λ_b, a larger λ_c results in lower values of $\mathcal{P}_b, \mathcal{P}_c, \mathcal{P}_d^H$ and $\mathcal{P}_d^F$, as shown in Fig. 6(a). This occurs because more transmissions from cellular devices can introduce additional interference to the transmissions of BSs, cellular devices and D2D devices, thereby decreasing their STPs.
- For a given λ_b, $\mathcal{P}_d^H$ and $\mathcal{P}_d^F$ are maximized when guard zones are set at both transmitting BSs and cellular devices, while they are minimized when no guard zones are implemented for either. Furthermore, $\mathcal{P}_b$ and $\mathcal{P}_c$ remain relatively unchanged, as illustrated in Fig. 6(b). This is because establishing guard zones reduces the activated probability of D2D devices p_a, leading to fewer D2D transmissions and thus increased $\mathcal{P}_d^H$ and $\mathcal{P}_d^F$, with negligible effects on $\mathcal{P}_b$ and $\mathcal{P}_c$.
- For a given λ_b, a larger P_d results in higher $\mathcal{P}_d^H$ and $\mathcal{P}_d^F$; conversely, a larger P_d leads to lower $\mathcal{P}_b$ and $\mathcal{P}_c$, as shown in Fig. 6(c). This occurs because a higher P_d correlates with increased received desired signal power at the D2D device, enhancing $\mathcal{P}_d^H$ and $\mathcal{P}_d^F$. However, a larger P_d also increases the undesired interference power received by the BSs and cellular devices, thus reducing $\mathcal{P}_b$ and $\mathcal{P}_c$.

5.5. Summary and Insights

Summary: All simulation results closely align with the theoretical ones, thus validating the accuracy of our analytical modeling[5]. From the results, we summarize three key observations below.

- *Dense Coexistence of Cellular and D2D Devices*: Increasing the density of BSs improves the STPs for both BSs and cellular devices.
- *Guard Zones Around BSs and Cellular Devices*: Expanding the radii of the two types of guard zones enhances the STP of D2D devices.
- *HD/FD Mode Selection*: Reducing the probability of D2D devices operating in FD mode increases their STP.

Insights: Based on the above observations, our analytical modeling can assist practitioners, such as network operators or engineers, in estimating the practical performance of SAGINs. For instance, it allows for configuring key network parameters—including the density of deployed BSs, the radii of the two types of guard zones, and the probability of D2D devices operating in full-duplex mode—across various application scenarios.

6. Conclusion and Discussions

6.1. Conclusion

The HetIoT, integrating large-scale cellular and D2D devices, has become a foundational component for 5G/B5G networks. In the context of full-duplex D2D communications within HetIoT, guard zones are introduced around both

[5]The minor discrepancies between some simulation values and theoretical predictions can be attributed to the limited simulations region or number of iterations. These issues can be mitigated by either improving the simulation parameters or enhancing computational hardware.

transmitting BSs and cellular devices to mitigate interference between concurrent cellular and D2D transmissions. This paper presents a novel spatial distribution model that effectively captures the location randomness and interdependencies of cellular and D2D devices. Using this model, it develops an analytical model to derive the expressions for the STPs of BSs, cellular, and D2D devices, accounting for the inherent randomness and interrelations between cellular and D2D transmissions, while also characterizing the complex mutual interference resulting from the two types of guard zones. Extensive Monte Carlo simulations validate the high accuracy of the proposed theoretical model. In future work, this modeling can be further explored to identify optimal parameter configurations, such as the radii of guard zones and the probability of D2D devices operating in FD mode, to enhance network performance.

6.2. Discussions

From the perspective of technical applications, our analytical modeling can integrate several emerging technologies into HetIoT, including mobile edge computing (MEC) [48, 49], edge artificial intelligence (AI) [50], and digital twin [51]. For instance, when deploying MEC within HetIoT, local model training involves a large number of edge IoT devices and requires efficient transmission of model updates. Our model can be utilized to analyze transmission performance, providing insights that guide suitable parameter configurations to enhance efficiency and reliability in MEC environments. Similarly, the integration of edge AI in HetIoT applications necessitates rapid and reliable data exchange for real-time decision-making and adaptive learning. Our modeling can help assess the communication performance between distributed edge devices and identify suitable network parameters, such as device density and transmission power, to support low-latency AI tasks effectively. In the case of digital twin technology, HetIoT facilitates real-time mirroring of physical assets in the digital world, which requires high-throughput and low-latency data transmission. Our model can assist in analyzing the required network configurations to ensure seamless data synchronization and reliable communication between the physical and virtual layers, thereby enhancing the accuracy and responsiveness of digital twins.

By applying our analytical modeling, practitioners can optimize HetIoT deployments to support these advanced technologies, thereby unlocking new possibilities for industrial automation, intelligent transportation, and other IoT-driven domains.

CRediT authorship contribution statement

Yulei Wang: Conceptualization, Methodology, Formal analysis, Software, Validation, Writing–original draft, Writing–review & editing. **Li Feng:** Supervision, Writing–review & editing, Project administration, Funding acquisition. **Yalin Liu:** Supervision, Writing–review & editing. **Zhongjie Li:** Writing–review & editing.

Declaration of competing interest

The authors declare that they have no known competing financial interests or personal relationships that could have appeared to influence the work reported in this paper.

Data Availability

The data underlying the results presented in the study are available within the paper.

Acknowledgments

The authors would like to thank the editor and anonymous reviewers for their valuable suggestions and insightful comments, which doubtlessly improved the quality of this paper and strengthened our contributions to the field.

References

[1] Q. Zhao, G. Li, J. Cai, M. Zhou, L. Feng, A tutorial on Internet of Behaviors: Concept, architecture, technology, applications, and challenges, IEEE Commun. Surv. Tutorials 25 (2023) 1227–1260. Doi:10.1109/COMST.2023.3246993.

[2] P. Borgohain, H. Choudhury, A lightweight D2D authentication protocol for relay coverage scenario in 5G mobile network, Comput. Networks 225 (2023) 109679. Doi:10.1016/J.COMNET.2023.109679.

[3] S. S. Sarma, R. Hazra, P. Goswami, Power optimization in a multicell D2D communication for smart city in an mm-wave cellular network: An mIoT perspective, IEEE Internet Things J. 10 (2023) 18686–18694. Doi:10.1109/JIOT.2023.3262577.

[4] T. Qiu, N. Chen, K. Li, M. Atiquzzaman, W. Zhao, How can heterogeneous Internet of Things build our future: A survey, IEEE Commun. Surv. Tutorials 20 (2018) 2011–2027. Doi:10.1109/COMST.2018.2803740.

[5] S. Feng, X. Lu, K. Zhu, D. Niyato, P. Wang, Covert D2D communication underlaying cellular network: A system-level security perspective, IEEE Trans. Wirel. Commun. 23 (2024) 9518–9533. Doi:10.1109/TWC.2024.3363186.

[6] L. Feng, Y. Liu, J. Guo, Y. Chen, Predicting impact of hitchhike on coexisted heterogeneous IoT networks, Appl. Soft Comput. 110 (2021) 107741. Doi:10.1016/j.asoc.2021.107741.

[7] L. Nie, X. Wang, Q. Zhao, Z. Shang, L. Feng, G. Li, Digital twin for transportation big data: a reinforcement learning-based network traffic prediction approach, IEEE Trans. Intell. Transp. Syst. 25 (2023) 896–906. Doi:10.1109/TITS.2022.3232518.

[8] K. Xu, Y. Qu, K. Yang, A tutorial on the internet of things: from a heterogeneous network integration perspective, IEEE Netw. 30 (2016) 102–108. Doi:10.1109/MNET.2016.7437031.

[9] A. Sørensen, H. Wang, M. J. Remy, N. Kjettrup, R. B. Sørensen, J. J. Nielsen, P. Popovski, G. C. Madueño, Modeling and experimental validation for battery lifetime estimation in NB-IoT and LTE-M, IEEE Internet of Things Journal 9 (2022) 9804–9819. Doi:10.1109/JIOT.2022.3152173.

[10] Y. Liu, Y. Deng, N. Jiang, M. Elkashlan, A. Nallanathan, Analysis of random access in NB-IoT networks with three coverage enhancement groups: A stochastic geometry approach, IEEE Trans. Wirel. Commun. 20 (2020) 549–564. Doi:10.1109/TWC.2020.3026331.

[11] S. Yao, L. Feng, Q. Zhao, Q. Yang, Y. Liang, ERFR-CTC: Exploiting residual frequency resources in physical-level cross-technology communication, IEEE Internet Things J. 8 (2020) 6062–6076. Doi:10.1109/JIOT.2020.3035692.

[12] M. Bembe, A. Abu-Mahfouz, M. Masonta, T. Ngqondi, A survey on low-power wide area networks for IoT applications, Telecommunication Systems 71 (2019) 249–274. Doi:10.1007/s11235-019-00557-9.

[13] K. S. Ali, H. ElSawy, M.-S. Alouini, Modeling cellular networks with full-duplex D2D communication: A stochastic geometry approach, IEEE Trans. Commun. 64 (2016) 4409–4424. Doi:10.1109/TCOMM.2016.2601912.

[14] S. Badri, M. Rasti, Interference management and duplex mode selection in in-band full duplex D2D communications: A stochastic geometry approach, IEEE Trans. Mob. Comput. 20 (2020) 2212–2223. Doi:10.1109/TMC.2020.2977899.

[15] C. Du, L. Xie, Z. Xing, J. An, Z. Zhang, Self-interference cancelation-based workload-driven duplex-model selection in machine-type communication networks, IEEE Internet Things J. 9 (2022) 20189–20202. Doi:10.1109/JIOT.2022.3172961.

[16] K. Ashfaq, G. A. Safdar, Uplink resource shared interference mitigation scheme for in-band D2D underlay 5G networks, Phys. Commun. 64 (2024) 102369. Doi:10.1016/j.phycom.2024.102369.

[17] M. Chu, A. Liu, J. Chen, V. K. Lau, S. Cui, A stochastic geometry analysis for energy-harvesting-based device-to-device communication, IEEE Internet Things J. 9 (2021) 1591–1607. Doi:10.1109/JIOT.2021.3091723.

[18] M. Haenggi, Stochastic geometry for wireless networks, Cambridge University Press, 2012.

[19] D. Stoyan, W. S. Kendall, S. N. Chiu, J. Mecke, Stochastic geometry and its applications, John Wiley & Sons, 2013.

[20] L. Chen, N. Deng, H. Wei, Performance analysis of D2D and cellular coexisting networks with interference management, IEEE Access 8 (2020) 82747–82759. Doi:10.1109/ACCESS.2020.2991077.

[21] R. Sun, H. Wu, B. Yang, Y. Shen, W. Yang, X. Jiang, T. Taleb, On covert rate in full-duplex D2D-enabled cellular networks with spectrum sharing and power control, IEEE IEEE Trans. Mob. Comput. 23 (2024) 9931–9945. Doi:10.1109/TMC.2024.3371377.

[22] Q. Guo, F. Tang, N. Kato, Federated reinforcement learning-based resource allocation in D2D-enabled 6G, IEEE Netw. 37 (2022) 89–95. Doi:10.1109/MNET.122.2200102.

[23] Y. Cai, S. Jin, W. Yu, X. Nie, L. Liang, H. Liu, Cooperative distributed resource allocation in heterogeneous networks with D2D communication, IEEE Trans. Veh. Technol. 72 (2023) 16426–16440. Doi:10.1109/TVT.2023.3290258.

[24] J. Sun, T. Liu, X. Wang, C. Xing, H. Xiao, A. V. Vasilakos, Z. Zhang, Optimal mode selection with uplink data rate maximization for D2D-aided underlaying cellular networks, IEEE Access 4 (2016) 8844–8856. Doi:10.1109/ACCESS.2016.2631243.

[25] J. Huang, J. Zou, C.-C. Xing, Energy-efficient mode selection for D2D communications in cellular networks, IEEE Trans. Cogn. Commun. Netw. 4 (2018) 869–882. Doi:10.1109/TCCN.2018.2873004.

[26] D. Torrieri, M. C. Valenti, Exclusion and guard zones in DS-CDMA ad hoc networks, IEEE Trans. Commun. 61 (2013) 2468–2476. Doi:10.1109/TCOMM.2013.041113.120714.

[27] E. Demarchou, C. Psomas, I. Krikidis, Asynchronous ad hoc networks with wireless powered cognitive communications, IEEE Trans. Cogn. Commun. Netw. 5 (2019) 440–451. Doi:10.1109/TCCN.2019.2908855.

[28] J. Park, I. Guvenc, Interference analysis for UAV radar networks with guard zones based on stochastic geometry, IEEE Trans. Aerosp. Electron. Syst. 59 (2023) 4092–4104. Doi:10.1109/TAES.2023.3236308.

[29] J. Ye, Y. J. Zhang, A guard zone based scalable mode selection scheme in D2D underlaid cellular networks, in: 2015 IEEE International Conference on Communications (ICC), IEEE, 2015, pp. 2110–2116. Doi:10.1109/ICC.2015.7248637.

[30] Z. Chen, M. Kountouris, Decentralized opportunistic access for D2D underlaid cellular networks, IEEE Trans. Commun. 66 (2018) 4842–4853. Doi:10.1109/TCOMM.2018.2834905.

[31] W. Shi, Z. Zhang, Y. Huang, W. Xu, Analysis of D2D-aided underlaying uplink cellular networks using Poisson hole process, IEEE Access 9 (2021) 12521–12532. Doi:10.1109/ACCESS.2021.3051385.

[32] A. H. Sakr, E. Hossain, Cognitive and energy harvesting-based D2D communication in cellular networks: Stochastic geometry modeling and analysis, IEEE Trans. Commun. 63 (2015) 1867–1880. Doi:10.1109/TCOMM.2015.2411266.

[33] H. Chen, L. Liu, H. S. Dhillon, Y. Yi, QoS-aware D2D cellular networks with spatial spectrum sensing: A stochastic geometry view, IEEE Trans. Commun. 67 (2018) 3651–3664. Doi:10.1109/TCOMM.2018.2889246.

[34] X. Zhang, J. G. Andrews, Downlink cellular network analysis with multi-slope path loss models, IEEE Trans. Commun. 63 (2015) 1881–1894. Doi:10.1109/TCOMM.2015.2413412.

[35] Y. Wang, Q. Zhao, S. Yao, M. Zhou, L. Feng, P. Zhang, Analytical modeling of location and contention randomness for node-assisted WiFi backscatter communication, IEEE Internet Things J. 11 (2024) 23336–23347. Doi:10.1109/JIOT.2024.3384032.

[36] Y. Liu, H.-N. Dai, M. Imran, N. Nasser, Ground-to-UAV communication network: Stochastic geometry-based performance analysis, in: ICC 2021-IEEE International Conference on Communications, IEEE, 2021, pp. 1–6. Doi:10.1109/ICC42927.2021.9500746.

[37] Y. Liu, H.-N. Dai, N. Zhang, Connectivity analysis of UAV-to-satellite communications in non-terrestrial networks, in: 2021 IEEE Global Communications Conference (GLOBECOM), IEEE, 2021, pp. 1–6. Doi:10.1109/GLOBECOM46510.2021.9685811.

[38] Y. Wang, Q. Zhao, S. Yao, L. Feng, H. Liang, Performance modeling of tags-to-WiFi transmissions for contention-based WiFi backscatter networks, in: 2022 IEEE International Conference on Networking, Sensing and Control (ICNSC), IEEE, 2022, pp. 1–6. Doi:10.1109/ICNSC55942.2022.10004070.

[39] L. Zhou, W. Pu, Y. Jiang, M.-Y. You, R. Zhang, Q. Shi, Joint optimization of UAV deployment and directional antenna orientation for multi-UAV cooperative sensing system, IEEE Trans. Wirel. Commun. 23 (2024) 14052–14065. Doi:10.1109/TWC.2024.3407837.

[40] S. D. Okegbile, B. T. Maharaj, A. S. Alfa, Interference characterization in underlay cognitive networks with intra-network and inter-network dependence, IEEE Trans. Mob. Comput. 20 (2020) 2977–2991. Doi:10.1109/TMC.2020.2993408.

[41] Y. Qin, M. A. Kishk, M.-S. Alouini, A dominant interferer plus mean field-based approximation for SINR meta distribution in wireless networks, IEEE Trans. Commun. 71 (2023) 3663–3678. Doi:10.1109/TCOMM.2023.3255907.

[42] Y. Qin, M. A. Kishk, M.-S. Alouini, On the downlink SINR meta distribution of UAV-assisted wireless networks, IEEE Trans. Commun. 71 (2023) 6762–6778. Doi:10.1109/TCOMM.2023.3305462.

[43] Y. Qin, M. A. Kishk, M.-S. Alouini, On the uplink SINR meta distribution of UAV-assisted wireless networks, IEEE Wirel. Commun. Lett. 12 (2023) 684–688. Doi:10.1109/LWC.2023.3239264.

[44] Q. Wang, H.-N. Dai, O. Georgiou, Z. Shi, W. Zhang, Connectivity of underlay cognitive radio networks with directional antennas, IEEE Trans. Veh. Technol. 67 (2018) 7003–7017. Doi:10.1109/TVT.2018.2825379.

[45] Q. Wang, Y. Zhou, H.-N. Dai, G. Zhang, W. Zhang, Performance on cluster backscatter communication networks with coupled interferences, IEEE Internet Things J. 9 (2022) 20282–20294. Doi:10.1109/JIOT.2022.3174002.

[46] D. Zwillinger, A. Jeffrey, Table of integrals, series, and products, Elsevier, 2007.

[47] P. Marrone, Exploring Device-to-Device (D2D) Communication in Cellular Technology: 5G and Beyond, Ph.D. thesis, Politecnico di Torino, 2024.

[48] Y. Fu, Y. Zhang, Q. Zhu, H.-N. Dai, M. Li, T. Q. Quek, A new vision of wireless edge caching networks (WECNs): Issues, technologies, and open research trends, IEEE Netw. 38 (2023) 247–253. Doi:10.1109/MNET.124.2200003.

[49] Y. Fu, Y. Shan, Q. Zhu, K. Hung, Y. Wu, T. Q. Quek, A distributed microservice-aware paradigm for 6G: Challenges, principles, and research opportunities, IEEE Netw. 38 (2023) 163–170. Doi:10.1109/MNET.2023.3321528.

[50] X. Xu, B. Xu, S. Han, C. Dong, H. Xiong, R. Meng, P. Zhang, Task-oriented and semantic-aware heterogeneous networks for artificial intelligence of things: Performance analysis and optimization, IEEE Internet Things J. 11 (2023) 228–242. Doi:10.1109/JIOT.2023.3305011.

[51] L. Chen, S. Zheng, Y. Wu, H.-N. Dai, J. Wu, Resource and fairness-aware digital twin service caching and request routing with edge collaboration, IEEE Wirel. Commun. Lett. 12 (2023) 1881–1885. Doi:10.1109/LWC.2023.3298200.

Yulei Wang received the B.S. degree from the University of Science and Technology Beijing, Beijing, China, in 2015, and the M.S. and Ph.D. degrees from Macau University of Science and Technology, Macau, China, in 2019 and 2024, respectively. Currently, he is affiliated with South-Central Minzu University, Wuhan, China, and is also a research assistant at Hong Kong Metropolitan University, Hong Kong, China. In 2015-2016, he was a senior data analyst at Institute of Social Science Survey, Peking University, Beijing, China. His current research interests include networking and wireless communication, space-air-ground integrated networks, and stochastic geometry.

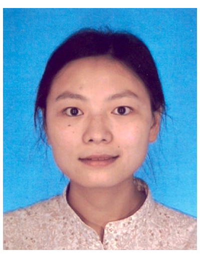

Li Feng received her M.S. degree in operation research from the Department of Mathematics, University of Hong Kong, Hong Kong, in 2007, and her Ph.D. degree in electronic information technology from the School of Computer Science and Engineering (SCSE), Macau University of Science and Technology (MUST), Macau, China, in 2013. She is currently an Associate Professor in SCSE, MUST. Her research interests include wireless and mobile networks, power saving, software defined networking, and performance analysis.

Yalin Liu received her Ph.D. degree from Macau University of Science and Technology in 2022. From January 2022 to May 2022, she worked as a research assistant at the Education University of Hong Kong. She is currently a lecturer at the School of Science and Technology, Hong Kong Metropolitan University. Her research interests include Space-Air-Ground Integrated Networks, Web 3.0, Stochastic Geometry, Large-Scale Network Modeling, and Network Optimization. Dr. Liu has served as a Technical Program Committee (TPC) member for conferences such as IEEE WCNC and IEEE VTC, and as a reviewer for various IEEE journals including IEEE IoT and IEEE Communication Magazine. She is also serving as a Co-guest Editor for MDPI Electronics.

Zhongjie Li received the B.S. and M.S. degrees in electronics and information engineering from Huazhong University of Science and Technology, China, in 1995 and 1998, respectively, and the Ph.D. degree in communication engineering from Nanyang Technological University, Singapore, in 2008. He is currently Professor with the School of Electronics and Information Engineering, South-Central Minzu University. His research interests include modeling and analyzing wireless networks, network optimization, and communication theory.